Blood-flow Volume Estimation by a 2-D Sparse Array

Giangrossi, Claudio; Ramalli, Alessandro; Guidi, Francesco; Noothout, Emile; Wei, Luxi; Vos, Hendrik J.; Tortoli, Piero

DOI
10.1016/j.ultrasmedbio.2025.06.005

Publication date
2025

Document Version
Final published version

Published in
Ultrasound in Medicine and Biology

Citation (APA)
Giangrossi, C., Ramalli, A., Guidi, F., Noothout, E., Wei, L., Vos, H. J., & Tortoli, P. (2025). Blood-flow Volume Estimation by a 2-D Sparse Array. *Ultrasound in Medicine and Biology*, *51*(9), 1580-1588. https://doi.org/10.1016/j.ultrasmedbio.2025.06.005

Ultrasound in Medicine & Biology 51 (2025) 1580–1588

Contents lists available at ScienceDirect

Ultrasound in Medicine & Biology

journal homepage: www.elsevier.com/locate/ultrasmedbio

Original Contribution

Blood-flow Volume Estimation by a 2-D Sparse Array

Claudio Giangrossi [a,*], Alessandro Ramalli [a], Francesco Guidi [a], Emile Noothout [b], Luxi Wei [c], Hendrik J. Vos [b,c], Piero Tortoli [a]

[a] Department of Information Engineering, University of Florence, Florence, Italy
[b] Department of Imaging Physics, Delft University of Technology, Delft, The Netherlands
[c] Department of Cardiology, Erasmus MC University Medical Center, Rotterdam, The Netherlands

ARTICLE INFO

Keywords:
Blood-flow volume
Bi-plane imaging
3-D imaging
High frame rate
Color flow mapping
Sparse array
Spiral array
ULA-OP 256

ABSTRACT

Objective: The assessment of blood-flow volume (BFV) is clinically relevant for the diagnosis and monitoring of cardiovascular dysfunctions and the prevention of subsequent secondary diseases. Non-invasive BFV measurement based on ultrasound methods are appealing for lower cost, real-time operation, and equipment portability. Recently, complex ultrasound research scanners with 1024 channels controlling the elements of a 2-D matrix array probe, have been demonstrated suitable for *off-line* accurate BFV estimates. In this work, a streamlined approach, using a 256-channel research scanner paired with a 256-element 2-D sparse spiral array, is proposed and validated.

Methods: This setup allows for simultaneous scanning of the vessel's longitudinal and transverse sections through an interleaved transmission sequence. In real-time, the longitudinal scan is used to determine the flow direction, while the transverse scan captures both the dynamic cross-sectional area and the local velocities by high frame rate color flow mapping.

Results: Flow phantom experiments under steady and pulsatile flow conditions were conducted to assess the performance by comparing the measurements with the outputs of a reference flow sensor. The proposed method provided accurate and precise BFV values for both flow conditions, with mean percentage error and standard deviation always lower than 9.4% and 2.8%, respectively. Furthermore, preliminary *in vivo* experiments have produced results consistent with those reported in the literature.

Conclusion: The proposed method based on the use of a sparse array has permitted accurate and precise phantom BFV measurements and has been shown suitable for real-time arterial BFV measurements.

Introduction

The assessment of arterial blood-flow volume (BFV) can reveal potential flow alterations caused by conditions such as atherosclerosis [1–6], vascular obstructions, neonatal aging, or fetal growth restriction [7,8]. In elderly individuals, changes in BFV over time may predict secondary diseases, such as vascular dementia and ischemic stroke, which impacts both quality and expectancy of life [1,9–11]. When measured in the common carotid arteries, BFV can evaluate the hemodynamic effects of stenosis and monitor cerebral blood-flow following carotid endarterectomy or carotid stenting stenosis [12,13].

Although phase contrast magnetic resonance imaging (MRI) angiography remains the gold standard for non-invasive BFV measurement [14–17], ultrasound methods are increasingly attractive for their low-cost, bedside feasibility, and real-time operation [18]. This has led many researchers to explore BFV assessment using a combination of ultrasound B-Mode images and pulsed Doppler techniques [19,20]. Typically, the vessel was scanned longitudinally, with the cross-section assumed to be circular, and the diameter measured as the distance between the vessel walls. The spatially averaged mean velocity was estimated either through uniform vessel sonication [21,22] or, assuming a fully developed velocity profile, from the time-averaged peak velocity [23–26]. However, these assumptions are not always valid, even in healthy common carotid arteries [27,28], and deviations can produce significant measurement errors [20]. Improved accuracy is achieved by extending the velocity estimation to an entire line crossing the vessel axis in a longitudinal vessel view, and using mean frequency [29–31] or multi-gate spectral Doppler [32] methods. Nevertheless, the following assumptions remain: A#1: the arterial lumen is cylindrical, that is, with a circular cross-section; A#2: the flow is parallel to the vessel wall; A#3: the flow has an axisymmetric profile.

An effective approach to eliminate any aprioristic assumption about flow distribution in a vessel is represented by three-dimensional (3-D)

* Corresponding author. Department of Information Engineering, University of Florence, Florence, Italy.
E-mail address: claudio.giangrossi@unifi.it (C. Giangrossi).

https://doi.org/10.1016/j.ultrasmedbio.2025.06.005
Received 12 December 2024; Revised 30 May 2025; Accepted 4 June 2025

vector flow imaging [33–35] techniques, which involve a significant increase in the ultrasound system complexity, processing load and time. In [36], Correia et al. estimated a volumetric blood-flow distribution through 2-D tilted plane-wave sonication, 2-D multi-angle cross-beam beamforming, and 3-D vector Doppler velocity components calculation by least-squares fitting. However, high volume rates (>4000 volumes/s) were achieved offline, with long computation times, using a 1024-channel scanner and a 1024-element matrix-array transducer. A possible way to limit the impact of above assumptions (A#1-A#3) without needing an extremely complex ultrasound system, is based on the investigation of the vessel of interest over a cross-sectional area. Although, in this case, the only assumption to be made would be A#3 (*i.e.*, that flow is parallel to the vessel wall) the cross-sectional view does not allow directly determining the (Doppler) angle between the ultrasound propagation direction and blood velocity. An example of method exploiting the cross-section view was proposed in reference [37]. By adding the assumption, A#1 (*i.e.*, cylindrical lumen), the authors proposed to determine the Doppler angle based on the elliptical intersection between the vessel and the ultrasound scan plane and demonstrated that, for Doppler angles below 70°, imaging the vessel cross-sectionally is more robust to motion and less operator-dependent than using longitudinal measurements.

In this work, a streamlined approach, first proposed in [38], is experimentally validated through flow phantom tests as well as *in vivo*. The novel method is based on a 256-element 2-D sparse spiral array [39] coupled to a 256-channel research scanner [40]. The 2-D array was exploited to simultaneously scan two orthogonal planes (bi-plane imaging): the longitudinal scan was used to estimate the beam-to-vessel angle by identifying the vessel walls through an accurate wall-tracking algorithm (WTA) [41,42]; the same algorithm was used to identify the vessel walls in the cross-sectional B-Mode image, thus allowing to set a contour for the detection of flow velocities through high frame rate (HFR) color flow mapping (CFM) [43]. The technique was validated by flow phantom tests under both steady and pulsatile flow conditions, as well as *in vivo* on the common carotid arteries of two volunteers. This demonstrates the capability of measuring flow in real-time using hardware that is significantly simpler than that employed in studies such as [36] and highlights the potential of the method for clinical applications such as non-invasive monitoring of blood flow in major arteries, early detection of vascular abnormalities, and assessment of hemodynamic responses in physiological studies.

The paper is organized as follows. The *Methods* section describes the proposed ultrasound BFV assessment technique and the setup used for phantom experimental tests. The outcomes for both steady and pulsatile flow are reported in the *Experimental results* section and discussed in the subsequent section. Finally, the *Conclusion* outlines key findings and introduces possible perspectives.

Methods

Bi-plane BFV measurement

BFV measurements quantify the blood volume flowing through a vessel per unit of time. It can be calculated by the surface integration of the blood velocity components perpendicular to the vessel cross-section S. If the flow velocities are non-invasively assessed through Doppler techniques, the BFV can be estimated by the following surface integral:

$$BFV = \iint_S v(x,z)\cdot dS \tag{1}$$

in which:

$$v(x,z) = \frac{f_d(x,z)\cdot c}{2f_0\cdot\cos\vartheta} \tag{2}$$

with f_0 the ultrasound frequency, $f_d(x,z)$ the 2-D map of the mean Doppler shifts, ϑ the Doppler angle (assumed to be constant over S), and c the ultrasound propagation speed. Accordingly, to achieve reliable BFV estimates, $f_d(x,z)$, S and ϑ must be accurately assessed.

The ultrasound system was programmed to scan two perpendicular planes covering the longitudinal- and the cross-section of the vessel, respectively. Both longitudinal and cross-sectional B-Mode images were obtained through focused, line-by-line sequences. These focused beams were interleaved with the transmission of diverging waves over the vessel cross-section, which are exploited to produce color flow maps at HFR.

The processing stages to extract the BFV are sketched in Figure 1. The cross-sectional B-Mode and CFM frames were used to estimate S and $f_d(x,z)$, respectively (Fig. 1, blocks 1 and 2). In the B-Mode images, the positions of the vessel walls were segmented, in real-time, through a WTA [41,42] (Fig. 1, blocks 2 and 3). Specifically, for both B-mode frames, the operator selects one initialization point inside the lumen. Then, the software automatically generates:

- On the longitudinal section, two 8-mm-long, 16-point segments: one shallower and one deeper than the initialization point. This setup allows the WTA to effectively track both the proximal and distal walls [41,42].
- On the cross section, to approximate an initial position of the vessel wall position, a 90-point circumference is placed with an angular step of 4°. Such a choice allowed balancing segmentation accuracy with computational load.

For each point of the segments/circumference, the mass center of the first-order absolute central moment of the grayscale image is computed in a circular domain of about 1.2-mm radius [41,42,44]. The mass center position is used in an iterative procedure that is concluded when the

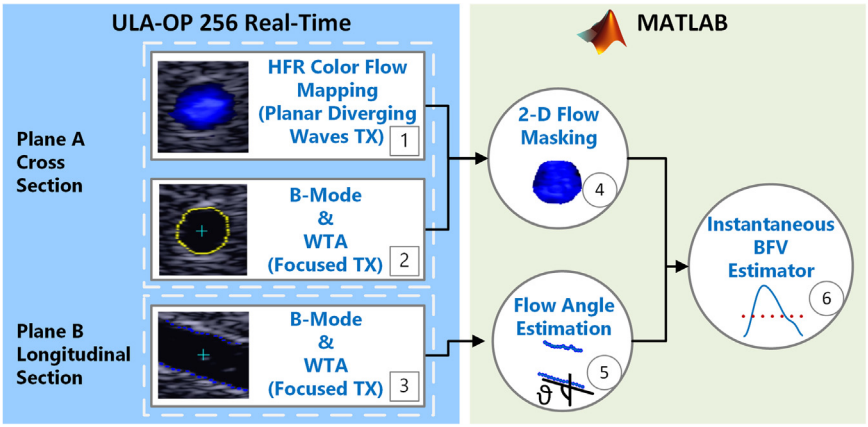

Figure 1. Processing stages of the proposed BFV estimation method. The realtime modules using wall tracking (WTA) and color flow mapping algorithms are shown on the left. The output data are either converted to files or streamed to a shared memory on the PC for offline or real-time MATLAB processing, respectively (right panel).

point converges to the wall of the vessel, that is, when, on two consecutive iterations, its position changes by less than 30 μm (a threshold heuristically set at a value much smaller than the wavelength).

The flow velocity maps, and the cross-sectional and longitudinal wall coordinates are, then, either saved to a file or streamed to a shared memory on the host personal computer (PC) to be offline or real-time post-processed, respectively, by a MATLAB (Version 2021b, The Math Works, Natick, MA, USA) script. In both cases, the script removes possible contributions from the region outside the vessel by masking the HFR color flow maps according to the time-varying cross-section segmentation (Fig. 1, block 4). The vessel orientation is calculated through a linear regression of the far wall coordinates (segmented on the longitudinal view). The latter option was preferred over other alternatives because, in our experience, the *in-vivo* segmentation of the far wall is less affected by artifacts due to multiple reflections on the intima, media, and adventitia, which may appear inside the vessel lumen close to the near wall. Fig. 1 block 5). The flow angle, ϑ, was estimated by assuming the flow parallel to the vessel walls. Finally, for each frame, the masked HFR color flow maps and the flow angle are combined to calculate the instantaneous BFV values according to eq. (1) (Fig. 1, block 6).

Experimental set-up

The ULA-OP 256 [40] is a programmable hardware-based research scanner suitable for the implementation of custom processing methods. The scanner, which has been shown capable of performing real-time 3-D HFR imaging [45,46], was here coupled to a 5-MHz prototype probe [47]. Specifically, 256 piezoelectric elements, sparsely distributed according to a spiral geometry over a 16-mm-diameter circular area, were wired to connectors through a printed circuit board. The number of probe elements thus matches the number of scanner channels.

As shown in Figure 2, a calibrated peristaltic pump (Watson-Marlow, Falmouth, UK) forced a blood-mimicking fluid to circulate, either in steady laminar or in pulsatile flow conditions, through a wall-less phantom. The phantom, manufactured by the University of Waterloo [48] on our design, was used to investigate two 7-mm diameter vessels located at depths of 20 and 40 mm, respectively. A thermal flow meter (TFM, Sensirion AG, Switzerland) provided the reference dynamic BFV values. For water flow, such values are guaranteed by the manufacturer with accuracy $\leq$5% in the range of 0–600 mL/min. However, a preliminary calibration using the blood-mimicking fluid allowed us to estimate accuracy better than $\pm$ 1% for average BFV measurements.

Scan sequences and imaging settings used in the experiments are summarized in Table 1. In all tests, the ULA-OP 256 was set to transmit Hamming-weighted 5-MHz 4-cycle sinusoidal bursts at PRF = 3.6 kHz. The beams scanned two perpendicular planes through an interleaved transmission sequence. B-Mode images were obtained by scanning 96

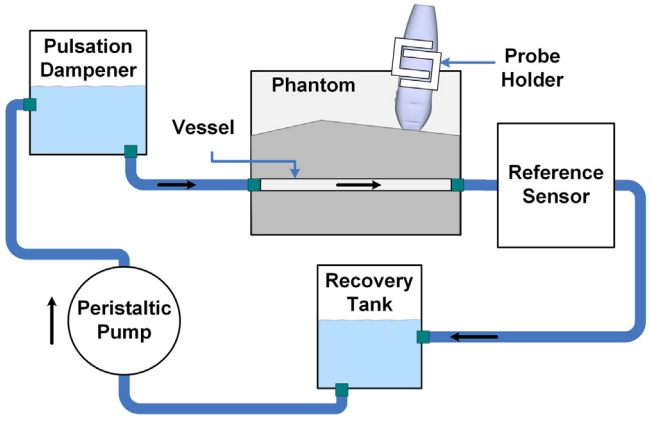

Figure 2. Experimental setup used in phantom tests. The peristaltic pump forces the circulation of the blood mimicking fluid in the phantom.

Table 1
scan sequences and imaging settings

Parameter	Value
Probe type	Sparse spiral array
Number of elements	256
TX Frequency	5 MHz
TX burst	4 sinusoidal cycles
PRF	3600 Hz
HFR CFM	
TX beam	Planar diverging Wave
Virtual source	-8.66 mm
Imaging lines	72
Sector opening angle	22.5°
Doppler PRF	1800 Hz
Ensemble Length	32
B-Mode	
TX beam	Focused beam line-by-line
Imaging lines	96 × 2
Sector opening angle	45°
PRF	1800 Hz

lines covering a 45° sector view, with beams focused on the vessel center depth in the cross-sectional view. The CFM cross-sectional frames were obtained by transmitting a beam diverging in the lateral direction but focused at the depth of the investigated vessel in the orthogonal direction; that is, a so-called planar diverging wave. The divergence was calculated by placing the virtual source at 8.66 mm behind the center of the probe aperture [46,49]. In reception, 72 lines covering a 22.5° sector were parallel beamformed by the ULA-OP 256 front-end circuits [50]. The wall filter was a continuous-time 4th order Chebyshev infinite impulse response filter, with 170 Hz cutoff frequency, corresponding to a velocity of 7 mm/s when the Doppler angle is 75°, as in most of our experiments. While this filter does not completely eliminate tissue motion, it significantly reduces its effects within the cross-section segmentation region that contributes to BFV estimates. The CFM module performed Doppler estimations through the algorithm described in detail in [43]. The ensemble length (EL) was here set equal to 32, suitable to produce high-quality Doppler maps even though diverging waves were transmitted. Since the Doppler sequence was interleaved with the B-Mode sequence, the final CFM frame rate was (PRF/2)/32 = 56 Hz, except when flows are characterized by extremely high pulsatility, such a frame rate looks sufficiently high to permit BFV estimations in large human arteries [51].

Data acquisition was guided by the ULA-OP 256 user interface (Fig. 3), which showed in real time the longitudinal- and cross-sectional B-Mode images (highlighting the calculated contours) of the vessel under investigation, as well as the cross-sectional color flow maps. Furthermore, the MATLAB live script allowed instantaneous feedback on the BFV trend.

Performance assessment

Steady and pulsatile flow experiments were performed to quantitatively assess the performance of the proposed method. In steady flow conditions, for each vessel depth (20 or 40 mm) and a 75° Doppler angle, six flow volumes between 100 and 600 mL/min were sequentially calibrated on the pump. In addition, the lower range flow values (100 −300 mL/min) were used for testing a 60° Doppler angle. In pulsatile flow conditions, the peristaltic pump was electronically driven by triangular waveforms having period and amplitude corresponding to 60 or 90 beats per minute (bpm) and flow volume peaks of 300, 400, or 500 mL/min, respectively. Due to limitations of the hydraulic system, particularly for the pump/pulsation dampener combination, the flow range (*i.e.*, the difference between maximum and minimum instantaneous flow) was here limited to 250 mL/min.

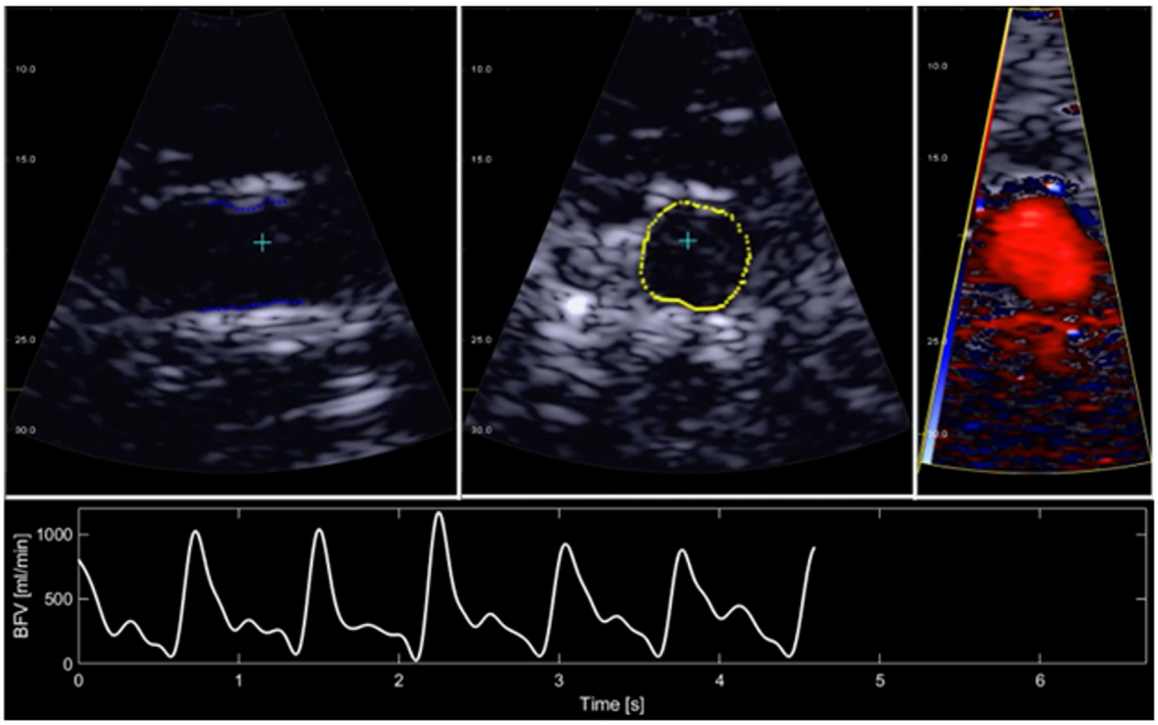

Figure 3. User interface of the ULA-OP scanner during an *in-vivo* experiment. Different views of the same common carotid artery are shown: B-Mode longitudinal (top-left) and cross- (top-center) section views, in which the tracked positions of the vessel walls are superimposed. The bottom panel shows the MATLAB real-time interface, providing the instantaneous BFV values.

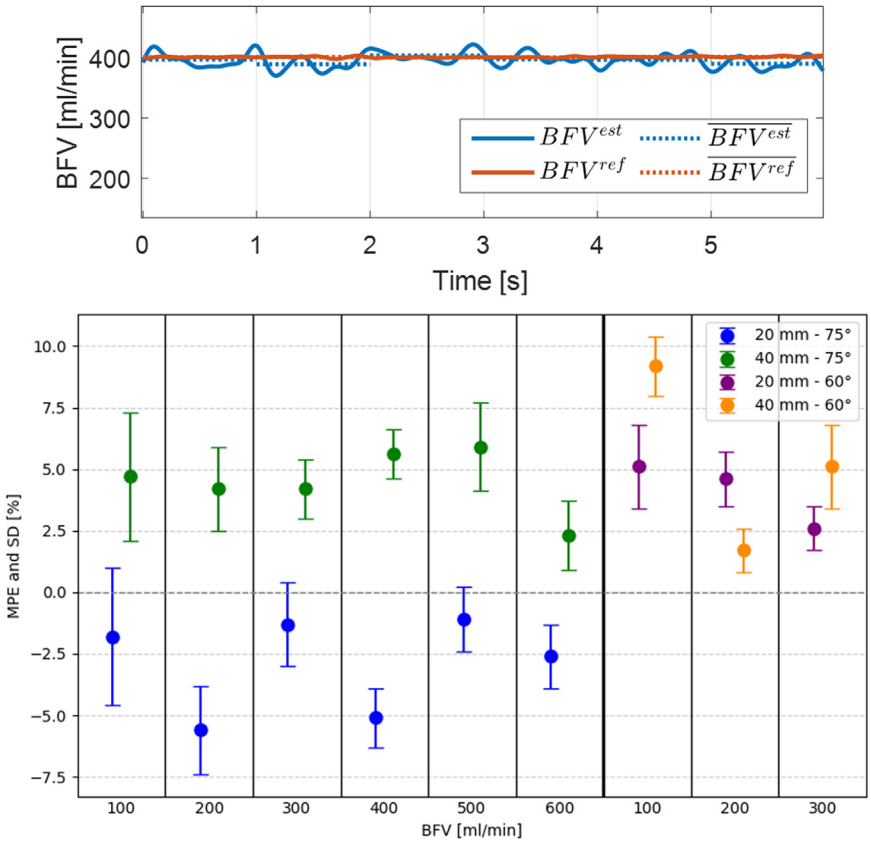

Figure 4. Top: Instantaneous trends of the BFV measured by the sensor and the ultrasound-based method during a steady flow experiment at 400 mL/min, 75° Doppler angle, and 40 mm depth. Bottom: mean percentage error (MPE) and standard deviation (SD) obtained for steady flow, different vessel depths and BFVs, at a 75° Doppler angle. The last 3 columns on the right report the results obtained at a 60° Doppler angle and different BFVs.

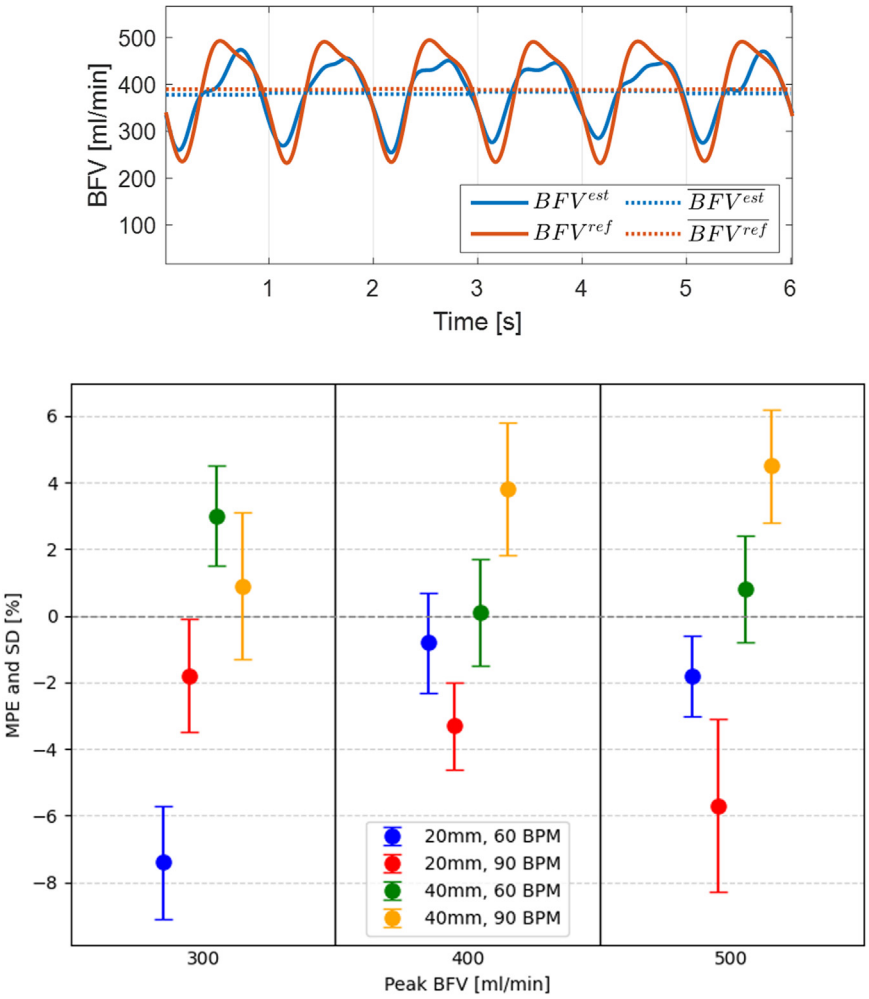

Figure 5. Top: Instantaneous trends of the BFV measured by the sensor and the ultrasound-based method during a pulsed flow experiment at 500 mL/min, 60 bpm and 20 mm vessel depth. The $\overline{BFV_n^{ref}}$ and $\overline{BFV_n^{est}}$ values, estimated per cycle, are shown in dotted lines. Bottom: mean percentage error (MPE) and standard deviation (SD) obtained for pulsatile flow, different vessel depths and BFVs at a 75° Doppler angle.

For each phantom setting, ten datasets, each 6-s long, were acquired. Each dataset was processed as described above to produce the estimated BFV values (BFV^{est}) to be compared to the reference values obtained through the sensor (BFV^{ref}). Specifically, the instantaneous BFV values were time-wise split into N blocks. For each (n-th) block, which was one-pulse-cycle long for a pulsatile flow and 1-s long for a steady flow, the reference ($\overline{BFV_n^{ref}}$) and estimated ($\overline{BFV_n^{est}}$) average BFV values were calculated. Finally, the mean percentage error (MPE) and standard deviation (SD) were obtained by:

$$MPE = \frac{1}{N}\sum_{n=1}^{N}\frac{\overline{BFV_n^{ref}} - \overline{BFV_n^{est}}}{\overline{BFV_n^{ref}}} \quad (3)$$

$$SD = \sqrt{\frac{1}{N}\sum_{n=1}^{N}\left|\frac{\overline{BFV_n^{ref}} - \overline{BFV_n^{est}}}{\overline{BFV_n^{ref}}} - MPE\right|^2} \quad (4)$$

Experimental results

Steady flow

Figure 4 (top) shows the results obtained for a sample dataset acquired in steady flow conditions at 400 mL/min. It shows that, although BFV^{est} is instantaneously more variable than BFV^{ref}, the block averaged values $\overline{BFV_n^{ref}}$ and $\overline{BFV_n^{est}}$ are quite similar. The same behavior was obtained for all datasets, depths of interest and volume flows. As summarized in Figure 4 (bottom), the MPE is in the range of (−6%; +9.4%) with SD between 1.0% and 2.8%.

Pulsatile flow

Figure 5 (top) shows the results obtained for a sample dataset acquired in pulsatile flow conditions for a peak of 500 mL/min at a pulse rate of 60 bpm and 20 mm depth. Equivalent results were obtained for the 40 mm investigation depth. Although BFV^{est} does not exactly follow the reference trend BFV^{ref}, the block averaged values $\overline{BFV_n^{ref}}$ and $\overline{BFV_n^{est}}$ are quite similar, as confirmed by the quantitative results summarized in Figure 5 (bottom). The MPE is between −7.4% and 4.5%, while the SD is between 1.2% and 2.6%.

In vivo

A preliminary *in-vivo* test was conducted to qualitatively evaluate the effectiveness of the method for human scanning. The test was conducted on the left common carotid artery of two healthy volunteers. The *in vivo* protocol was approved by the institutional review board on ethics of the University of Florence (approval number 309/2024) and informed consent was obtained from each volunteer.

Real-time imaging facilitated a correct probe positioning over the carotid. The real-time segmentation of the two vessel views, superimposed in yellow and blue dots to the two B-Mode views was manually started by the operator by positioning the blue cross in the vessel lumen. The real-time CFM display (right panel) supported the operator to detect the blood-flow. Once the region of interest was identified and the probe

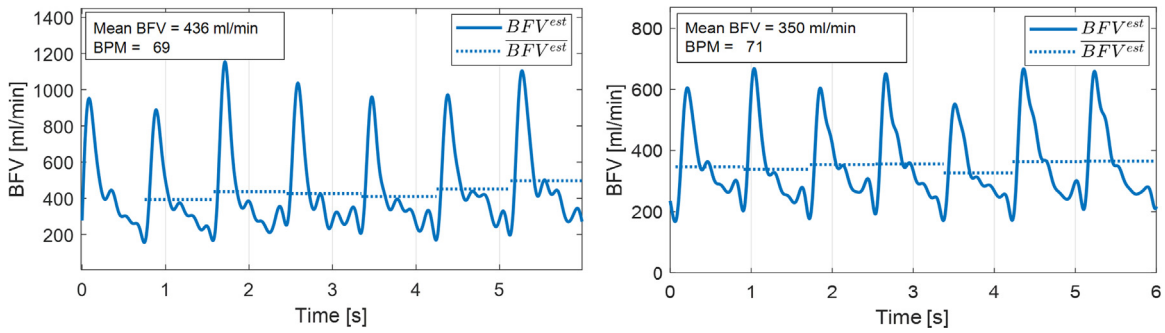

Figure 6. Instantaneous BFV values measured for two healthy volunteers.

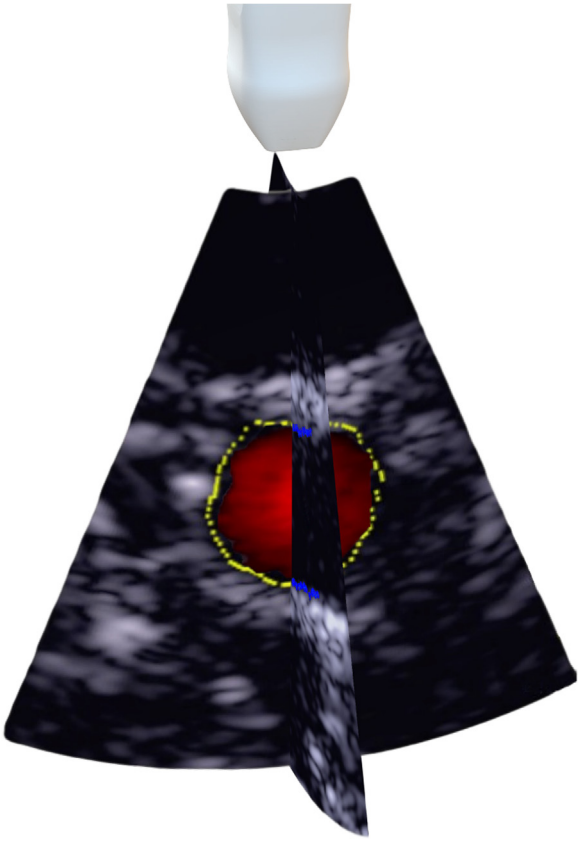

Figure 7. Overall pictorial representation of the biplane modality.

stably positioned (see Video 1, here attached as supplementary material), the volunteer was asked to hold his breath, and the operator could press a button to start the MATLAB live script for real-time assessment of the instantaneous BFV values and simultaneously acquire a 6-s long dataset. The acquired data could also be post-processed in MATLAB for detailed estimations producing BFV trends like those shown in Fig. 6. Both the BFV patterns follow a physiological trend, with clear dicrotic notches that well-separate the systolic and diastolic phases. The younger subject reported a pulsatile flow with 69 BPM and a mean BFV of 436 mL/min. For the older volunteer, 71 bpm and a mean BFV value of 350 mL/min were measured.

Discussion

A novel method for BFV measurements has been described and validated through accurate phantom and *in vivo* measurements. As pictorially illustrated in Figure 7, the method exploits bi-plane ultrasound scan performed with a 2-D sparse array probe. The longitudinal plane is used to determine the flow direction, while the transverse plane permits an accurate assessment of the time-varying cross-sectional area over which the velocity contributions are calculated. An important role was played by the WTA, which, in previous studies [42,44,52], provided satisfactory performance and no reliability issues. To achieve high temporal resolution, CFM was performed at a HFR. This was accomplished, in real-time, by transmitting planar diverging waves and exploiting the high-performance parallel beamformer onboard ULA-OP 256. This strategy allowed long ELs, so that good quality CFM images were obtained. In B-mode imaging, high temporal resolution and contrast were achieved by interleaving the transmission of planar diverging waves and focused waves. This has enabled the tracking algorithm to precisely follow the vessel wall movements throughout the cardiac cycle and accurately estimate the vessel area and flow angle. Compared to the preliminary work [38], the transmission strategy was modified to boost the BFV estimation rate and enhance the CFM spatial resolution by increasing the maps' pixel density inside the vessel. A higher frequency probe was also used to better resolve the vessel contour, and the experimental results were compared with a reference sensor recently included in the hydraulic circuit.

The measurements based on the proposed method are inevitably influenced by multiple potential sources of error. Inaccuracies in the WTA, caused by artifacts that might distort the 2-D flow masking, can occur. Even with an orthogonal view, small misalignment errors can lead to inaccuracies in the Doppler angle estimation. Also, the velocity calculation by the CFM algorithm is sensitive to white noise and tissue movements [51]. However, the use of a great EL (32), enabled by the HFR approach, helps counteract such a sensitivity by providing a more accurate estimation of the mean velocity and effective clutter attenuation. Figure 3 and the accompanying movie show that the CFM boundaries spill outside the vessel wall due to the worse spatial resolution achieved with planar diverging waves. Nevertheless, the good focusing capability of the B-mode beam ensures quite a good segmentation of the vessel boundaries, which is crucial to avoid considering flow contribution from outside of the vessel. Notwithstanding all such limitations, the steady flow experiments have shown excellent accuracy and precision, with MPE and SD always lower than 6% and 2.8%, respectively. The measurements done for the deeper vessel show a higher average MPE, which could be attributed to a lower signal-to-noise ratio and worse spatial resolution. The data for $\vartheta = 75°$ in Figures 4 and 5 indicate that the errors are negative at shallower depths and positive at greater depths. However, it is worth noting that when the Doppler angle is relatively high (75°), even a small estimation error (*e.g.*, ±1°) can result in a significant BFV error (*e.g.*, ±6% [37]). Since the probe was re-positioned before investigating a different vessel, it is possible that the angle estimation error was negative for one vessel and positive for the other. These errors could have been sufficiently high in both cases to be dominant and determine bias values with the same sign for all measurements at each depth. Additional steady flow measurements (results are reported in the three columns on the right) performed at 3 different BFVs and 60° Doppler angle, which is expected to be much less sensitive

Table 2
Qualitative comparison of BFV estimators

Method	Assumptions	Probe misalignment sensitivity	Hardware requirements / Real-time capability
Longitudinal scan + velocity estimation in a single sample volume [21–26]	A#1, A#2, A#3, and parabolic flow profile	The sample volume must intercept the peak flow velocity at the vessel's center	Low (PoC and portable scanners) / Yes
Longitudinal scan + velocity estimation along a line [29–32]	A#1, A#2, and A#3	The Doppler line must cross the vessel's axis	Low (PoC and portable scanners) / Yes
Longitudinal 2-D Vector Flow Imaging [54–57]	A#1, A#3, and neglectable out-of-plane velocity component	The scan plane must include the vessel's diameter	Moderate (mid-end scanners) / Yes
Cross-sectional scan + velocity estimation based on CFM [37]	A#1 and A#2	Elliptical intersection between the vessel and the ultrasound plane The Doppler angle must be low (<70°)	Moderate (mid-end scanners) / Feasible
Bi-plane B-Mode and cross-sectional HFR CFM [this work]	A#2	The longitudinal plane should align with any longitudinal section of the vessel	Moderate (mid-end scanners) / Yes
3D Vector Doppler Imaging [34–36]	None	None	High (high-end scanners) / No

A#1: the arterial lumen is cylindrical; A#2: the flow is parallel to the vessel wall; A#3: the flow has an axisymmetric profile.

to this issue, confirmed this hypothesis, showing errors with the same sign at both vessel depths (*e.g.*, 2.6% ± 0.9% at 20 mm and 5.1% ± 1.7% at 40 mm at 300 mL/min).

High measurement accuracy and repeatability were confirmed by pulsatile flow experiments. The MPE was lower than 7.4% and SD < 2.6% in all cases, even though the instantaneous values did not always closely follow the rapid flow variations highlighted by the sensor. The discrepancy between the two curves can be attributed to the different BFV measurement points. Specifically, ultrasound measurements were conducted at half length of the vessel phantom, while the sensor was placed at the outlet. It is worth noting that by comparing the BFV trends acquired with two sensors, placed at the inlet and the outlet of the phantom, respectively, the trend exhibited by the output sensor was found significantly more peaked. It is therefore reasonable to assume that the output trend was also more peaked than the trend within the vessel. This suggests that the curves detected by the proposed method well match the flow present in that specific section of the vessel. Finally, the peak and average BFV values measured during *in vivo* experiments are in good agreement with those obtained using conventional linear arrays [30,53] or dense 2-D probes [36]. However, *in vivo*, an additional source of error could be the presence of velocity components not parallel to the vessel wall, for example, due to the slight curvature of vessels like the common carotid artery [27]. Overall, the results confirm that the application of our method using sparse array technology for volumetric blood-flow measurements is indeed feasible. Despite the well-known loss of image contrast in morphological imaging, such technology allows using significantly simplified hardware compared to that required to drive dense 2-D probes. For example, in reference [36] a 1024-element matrix-array probe was driven by four synchronized Aixplorer systems (Supersonic Imagine, France). Furthermore, in [35,36] the flow velocities were estimated, with long post-processing times, through 3-D vector Doppler measurements.

For the readers' convenience, Table 2 provides a list of representative ultrasound methods adopted for BFV estimation. The Table highlights that the methods' evolution has yielded a reduction in the number of assumptions with a corresponding increase in hardware complexity. The possible use of two-dimensional (2-D) vector Doppler or speckle tracking techniques [54–57] just mitigates the assumption A#2, maintaining the hypothesis that the out-of-plane velocity component is neglectable. When this condition is satisfied, a good agreement between velocities detected by 2-D ultrasound vector Doppler methods and MRI-based techniques can be achieved [58,59]. However, to eliminate the assumption of axisymmetric flow profile, it is necessary to include a cross-sectional vessel scan. Compared to the method illustrated in [37], which reconstructs the cross-sectional image only, our approach does not assume a cylindrical vessel geometry and obtains good accuracy even for Doppler angles exceeding 70°. In both cases, the flow direction is assumed to be parallel to the vessel wall. While this assumption holds well for a straight-tube-phantom and the *in vivo* measurements presented here, it may not be valid in regions with disturbed or complex flow patterns, such as those found near vascular stenoses [60]. In such cases, BFV measurements should be performed upstream or downstream of the stenosis. For example, in the presence of stenosis at the carotid bifurcation, BFV measurements should be taken in the common or internal carotid artery [61,62]. Despite this limitation, the proposed framework is well-suited for application in major vessels where flow remains relatively uniform and aligned with the vessel axis. These include clinically relevant sites such as the abdominal aorta, femoral arteries, and segments of the carotid artery away from bifurcations or plaques. In these contexts, accurate and non-invasive BFV estimation can support the monitoring of peripheral artery disease, assessment of hemodynamic changes in response to interventions, or evaluation of cardiovascular risk [63–66].

To extend the clinical applicability of our method to more complex vascular regions, future work should incorporate advanced vector Doppler techniques, potentially in 3-D [34,67], to capture multi-directional flow components.

Conclusion

A method for ultrasound BFV measurements and its experimental validation for both steady and pulsatile flow have been presented. The method is based on bi-plane (B-mode and HFR CFM) imaging to simultaneously scan the cross- and longitudinal-section of the vessel under investigation. It is noteworthy that using the sparse array probe facilitates use and future exploitation. The proposed method is compatible with scanners including a limited (256) number of channels, is suitable for real-time implementation, can provide accurate and precise phantom BFV measurements, and is feasible for *in vivo* measurements.

The next activities will aim at a clinical validation of the proposed method by an extensive study on the common carotid arteries of healthy subjects and patients.

Conflict of interest

The authors declare no competing interests.

CRediT authorship contribution statement

Claudio Giangrossi: conceptualization, methodology, software, validation, writing—original draft, writing—review and editing. **Alessandro Ramalli:** Conceptualization, methodology, validation, writing—original draft, supervision, writing—review and editing. **Francesco Guidi:** methodology, software, writing—review and editing. **Emile Noothout:** resources, writing—review and editing. **Luxi Wei:** resources, writing—review and editing. **Hendrik J. Vos:** resources, writing—review and editing. **Piero Tortoli:** conceptualization, methodology, resources, writing—original draft, writing—review and editing, supervision.

Acknowledgments

The Department of Information Engineering, University of Florence, acknowledges the contribution of the PRIN 2020 project CONUS (CUP: B13C21000190005) under Grant 20205HFXE7, funded by the Italian Ministry of Education, University and Research. The work by HJV, LW and EN was supported by the research programme "Vernieuwingsimpuls – Vidi 2017" with project number QUANTO-16572, which is (partly) financed by the Dutch Research Council (NWO).

Data availability statement

The datasets of the current study are not publicly available due to volunteers' privacy but are available from the corresponding author upon reasonable request.

Supplementary materials

Supplementary material associated with this article can be found in the online version at doi:10.1016/j.ultrasmedbio.2025.06.005.

References

[1] Ackroyd N, Gill R, Griffiths K, Kossoff G, Appleberg M. Quantitative common carotid artery blood flow: prediction of internal carotid artery stenosis. J Vasc Surg 1986;3:846–53. doi: 10.1016/0741-5214(86)90148-5.
[2] Wada T, Kodaira K, Fujishiro K, Okamura T. Correlation of common carotid flow volume measured by ultrasonic quantitative flowmeter with pathological findings. Stroke 1991;22:319–23. doi: 10.1161/01.STR.22.3.319.
[3] Scheel P, Puls I, Becker G, Schöning M. Volume reduction in cerebral blood flow in patients with vascular dementia. Lancet 1999;354:2137. doi: 10.1016/S0140-6736(99)04016-7.
[4] Acar M, Degirmenci B, Yucel A, Albayrak R, Haktanir A. An evaluation of internal carotid artery and cerebral blood flow volume using color duplex sonography in patients with vertebral artery hypoplasia. Eur J Radiol 2005;53:450–3. doi: 10.1016/j.ejrad.2004.05.010.
[5] Han H, Zhang R, Liu G, Qiao H, Chen Z, Liu Y, et al. Reduction of cerebral blood flow in community-based adults with subclinical cerebrovascular atherosclerosis: a 3.0T magnetic resonance imaging study. NeuroImage 2019;188:302–8. doi: 10.1016/j.neuroimage.2018.12.021.
[6] Prussien KV, Compas BE, Siciliano R, Jones RS, Ciriegio AE, Lee CA, et al. Cerebral blood flow, brain volume, and age predicts executive function in sickle cell anemia. Blood 2021;138:976. doi: 10.1182/blood-2021-152504.
[7] Gardiner H, Brodszki J, Eriksson A, Marl K. Volume blood flow estimation in the normal and growth-restricted fetus. Ultrasound Med Biol 2002;28:1107–13. doi: 10.1016/S0301-5629(02)00565-3.
[8] Kehrer M, Krägeloh-Mann I, Goelz R, Schöning M. The development of cerebral perfusion in healthy preterm and term neonates. Neuropediatrics 2003;34:281–6. doi: 10.1055/s-2003-44663.
[9] Scheel P, Ruge C, Schöning M. Flow velocity and flow volume measurements in the extracranial carotid and vertebral arteries in healthy adults: reference data and the effects of age. Ultrasound Med Biol 2000;26:1261–6. doi: 10.1016/S0301-5629(00)00293-3.
[10] Venkat P, Chopp M, Chen J. Models and mechanisms of vascular dementia. Exp Neurol 2015;272:97–108. doi: 10.1016/j.expneurol.2015.05.006.
[11] Kaszczewski P, Elwertowski M, Leszczynski J, Ostrowski T, Galazka Z. Volumetric carotid flow characteristics in Doppler ultrasonography in healthy population over 65 years old. J Clin Med 2020;9:1375. doi: 10.3390/jcm9051375.
[12] Ho SSY, Chan YL, Yeung DKW, Metreweli C. Blood flow volume quantification of cerebral ischemia. Am J Roentgenol 2002;178:551–6. doi: 10.2214/ajr.178.3.1780551.
[13] Mitrasinovic A, Radak S, Kolar J, Aleksic N, Otasevic P, Popovic M, et al. Color Doppler sonographic evaluation of flow volume of the internal carotid and vertebral arteries after carotid endarterectomy. J Clin Ultrasound 2010;38:238–43. doi: 10.1002/jcu.20670.
[14] van Zijl PCM, Eleff SM, Ulatowski JA, Oja JME, Uluğ AM, Traystman RJ, et al. Quantitative assessment of blood flow, blood volume and blood oxygenation effects in functional magnetic resonance imaging. Nat Med 1998;4:159–67. doi: 10.1038/nm0298-159.
[15] Guo G, Yang Y, Yang W. Cerebral blood flow volume measurements of the carotid artery and ipsilateral branches using two-dimensional phase-contrast magnetic resonance angiography*☆. Neural Regen Res 2011;6:2367. doi: 10.3969/j.issn.1673-5374.2011.30.009.
[16] Markl M, Frydrychowicz A, Kozerke S, Hope M, Wieben O. 4D flow MRI. J Magn Reson Imaging 2012;36:1015–36. doi: 10.1002/jmri.23632.
[17] Muir ER, Watts LT, Tiwari YV, Bresnen A, Shen Q, Duong TQ. Quantitative cerebral blood flow measurements using MRI. In: Milner R, editor. Cerebral angiogenesis: methods and protocols. New York: Springer; 2014. p. 205–11. doi: 10.1007/978-1-4939-0320-7_17.
[18] Golemati S, Cokkinos DD. Recent advances in vascular ultrasound imaging technology and their clinical implications. Ultrasonics 2022;119:106599. doi: 10.1016/j.ultras.2021.106599.
[19] Hoskins PR. Haemodynamics and blood flow measured using ultrasound imaging. Proc Inst Mech Eng H 2010;224:255–71. doi: 10.1243/09544119JEIM572.
[20] Evans DH, McDicken WN. Doppler ultrasound: physics, instrumentation and signal processing. 2nd ed Chichester; New York: Wiley; 1999.
[21] Gill RW. Pulsed Doppler with B-Mode imaging for quantitative blood flow measurement. Ultrasound Med Biol 1979;5:223–35. doi: 10.1016/0301-5629(79)90014-0.
[22] Evans DH. Can ultrasonic duplex scanners really measure volumetric flow? In: Evans JA, editor. Physics in Medical Ultrasound. York: IPEM; 1986. p. 145–54.
[23] Li S, Hoskins PR, Anderson T, McDicken WN. Measurement of mean velocity during pulsatile flow using time-averaged maximum frequency of Doppler ultrasound waveforms. Ultrasound Med Biol 1993;19:105–13. doi: 10.1016/0301-5629(93)90002-6.
[24] Levine RL, Turski PA, Holmes KA, Grist TM. Comparison of magnetic resonance volume flow rates, angiography, and carotid Dopplers. Preliminary results. Stroke 1994;25:413–7. doi: 10.1161/01.STR.25.2.413.
[25] Holland CK, Clancy MJ, Taylor KJW, Alderman JL, Purushothaman K, McCauley TR. Volumetric flow estimation in vivo and in vitro using pulsed-Doppler ultrasound. Ultrasound Med Biol 1996;22:591–603. doi: 10.1016/0301-5629(96)00046-4.
[26] Ricci S, Matera R, Tortoli P. An improved Doppler model for obtaining accurate maximum blood velocities. Ultrasonics 2014;54:2006–14. doi: 10.1016/j.ultras.2014.05.012.
[27] Tortoli P, Michelassi V, Bambi G, Guidi F, Righi D. Interaction between secondary velocities, flow pulsation and vessel morphology in the common carotid artery. Ultrasound Med Biol 2003;29:407–15. doi: 10.1016/S0301-5629(02)00705-6.
[28] Manbachi A, Hoi Y, Wasserman BA, Lakatta EG, Steinman DA. On the shape of the common carotid artery with implications for blood velocity profiles. Physiol Meas 2011;32:1885–97. doi: 10.1088/0967-3334/32/12/001.
[29] Picot PA, Embree PM. Quantitative volume flow estimation using velocity profiles. IEEE Trans Ultrason Ferroelectr Freq Control 1994;41:340–5. doi: 10.1109/58.285468.
[30] Likittanasombut P, Reynolds P, Meads D, Tegeler C. Volume flow rate of common carotid artery measured by Doppler method and color velocity imaging quantification (CVI-Q). J Neuroimaging 2006;16:34–8. doi: 10.1177/1051228405001523.
[31] Kaszczewski P, Elwertowski M, Leszczyński J, Ostrowski T, Gałązka Z. Volumetric flow assessment in Doppler ultrasonography in risk stratification of patients with internal carotid stenosis and occlusion. J Clin Med 2022;11:531. doi: 10.3390/jcm11030531.
[32] Ricci S, Cinthio M, Ahlgren ÅR, Tortoli P. Accuracy and reproducibility of a novel dynamic volume flow measurement method. Ultrasound Med Biol 2013;39:1903–14. doi: 10.1016/j.ultrasmedbio.2013.04.017.
[33] Dunmire B, Beach KW, Labs K-H, Plett M, Strandness DE. Cross-beam vector Doppler ultrasound for angle-independent velocity measurements. Ultrasound Med Biol 2000;26:1213–35. doi: 10.1016/S0301-5629(00)00287-8.
[34] Holbek S, Ewertsen C, Bouzari H, Pihl MJ, Hansen KL, Stuart MB, et al. Ultrasonic 3-D vector flow method for quantitative in vivo peak velocity and flow rate estimation. IEEE Trans Ultrason Ferroelectr Freq Control 2017;64:544–54. doi: 10.1109/TUFFC.2016.2639318.
[35] Holbek S, Hansen KL, Bouzari H, Ewertsen C, Stuart MB, Thomsen C, et al. Common carotid artery flow measured by 3-d ultrasonic vector flow imaging and validated with magnetic resonance imaging. Ultrasound Med Biol 2017;43:2213–20. doi: 10.1016/j.ultrasmedbio.2017.06.007.
[36] Correia M, Provost J, Tanter M. M. Pernot, 4D ultrafast ultrasound flow imaging: in vivo quantification of arterial volumetric flow rate in a single heartbeat. Phys, Med, Biol 2016;61:L48. doi: 10.1088/0031-9155/61/23/L48.
[37] van Knippenberg L, van Sloun RJG, Shulepov S, Bouwman RA, Mischi M. An angle-independent cross-sectional Doppler method for flow estimation in the common carotid artery. IEEE Trans Ultrason Ferroelectr Freq Control 2020;67:1513–24. doi: 10.1109/TUFFC.2020.2975315.
[38] Giangrossi C, Ramalli A, De Cianni M, Guidi F, Tortoli P. Blood-flow volume estimation with bi-plane imaging. 2022 IEEE International Ultrasonics Symposium (IUS); 2022. p. 1–4. doi: 10.1109/IUS54386.2022.9957268.
[39] Ramalli A, Boni E, Savoia AS, Tortoli P. Density-tapered spiral arrays for ultrasound 3-D imaging. IEEE Trans Ultrason Ferroelectr Freq Control 2015;62:1580–8. doi: 10.1109/TUFFC.2015.007035.
[40] Boni E, Bassi L, Dallai A, Guidi F, Meacci V, Ramalli A, et al. ULA-OP 256: a 256-channel open scanner for development and real-time implementation of new ultrasound methods. IEEE Trans Ultrason Ferroelectr Freq Control 2016;63:1488–95. doi: 10.1109/TUFFC.2016.2566920.
[41] Demi M, Paterni M, Benassi A. The first absolute central moment in low-level image processing. Comput Vis Image Underst 2000;80:57–87. doi: 10.1006/cviu.2000.0861.
[42] Gemignani V, Faita F, Ghiadoni L, Poggianti E, Demi M. A system for real-time measurement of the brachial artery diameter in B-Mode ultrasound images. IEEE Trans Med Imaging 2007;26:393–404. doi: 10.1109/TMI.2006.891477.
[43] Guidi F, Tortoli P. Real-time high frame rate color flow mapping system. IEEE Trans Ultrason Ferroelectr Freq Control 2021;68:2193–201. doi: 10.1109/TUFFC.2021.3064612.
[44] Ramalli A, Aizawa K, Shore AC, Morizzo C, Palombo C, Lenge M, et al. Continuous simultaneous recording of brachial artery distension and wall shear rate: a new boost for flow-mediated vasodilation. IEEE Trans Ultrason Ferroelectr Freq Control 2019;66:463–71. doi: 10.1109/TUFFC.2018.2889111.
[45] Giangrossi C, Ramalli A, Dallai A, Mazierli D, Meacci V, Boni E, et al. Requirements and hardware limitations of high-frame-rate 3-D ultrasound imaging systems. Appl Sci 2022;12:6562. doi: 10.3390/app12136562.
[46] Ramalli A, Harput S, Bézy S, Boni E, Eckersley RJ, Tortoli P, et al. High-frame-rate triplane echocardiography with spiral arrays: from simulation to real-time

implementation. IEEE Trans Ultrason Ferroelectr Freq Control 2020;67:57–69. doi: 10.1109/TUFFC.2019.2940289.
[47] Wei L, Boni E, Ramalli A, Fool F, Noothout E, van der Steen AFW, et al. Sparse 2-D PZT-on-PCB arrays with density tapering. IEEE Trans Ultrason Ferroelectr Freq Control 2022;69:2798–809. doi: 10.1109/TUFFC.2022.3204118.
[48] Ho CK, Chee AJY, Yiu BYS, Tsang ACO, Chow KW, Yu ACH. Wall-less flow phantoms with tortuous vascular geometries: design principles and a patient-specific model fabrication example. IEEE Trans Ultrason Ferroelectr Freq Control 2017;64:25–38. doi: 10.1109/TUFFC.2016.2636129.
[49] Chen Y, Tong L, Ortega A, Luo J, D'hooge J. Feasibility of multiplane-transmit beamforming for real-time volumetric cardiac imaging: a simulation study. IEEE Trans Ultrason Ferroelectr Freq Control 2017;64:648–59. doi: 10.1109/TUFFC.2017.2651498.
[50] Meacci V, Boni E, Dallai A, Ramalli A, Scaringella M, Guidi F, et al. FPGA-based multi cycle parallel architecture for real-time processing in ultrasound applications. Lect Notes Electr Eng 2019;550:295–301. doi: 10.1007/978-3-030-11973-7_34.
[51] Evans DH, Jensen JA, Nielsen MB. Ultrasonic colour Doppler imaging. Interface Focus 2011;1:490–502. doi: 10.1098/rsfs.2011.0017.
[52] Aizawa K, Ramalli A, Sbragi S, Tortoli P, Casanova F, Morizzo C, et al. Arterial wall shear rate response to reactive hyperaemia is markedly different between young and older humans. J Physiol 2019;597:4151–63. doi: 10.1113/JP278310.
[53] Marshall I, Papathanasopoulou P, Wartolowska K. Carotid flow rates and flow division at the bifurcation in healthy volunteers. Physiol, Meas 2004;25:691. doi: 10.1088/0967-3334/25/3/009.
[54] Aoudi W, Liebgott H, Needles A, Yang V, Foster FS, Vray D. Estimation methods for flow imaging with high frequency ultrasound. Ultrasonics 2006;44:e135–40. doi: 10.1016/j.ultras.2006.06.025.
[55] Marion A, Aoudi W, Basarab A, Delachartre P, Vray D. Blood flow evaluation in high-frequency, 40 MHz imaging: a comparative study of four vector velocity estimation methods. Ultrasonics 2010;50:683–90. doi: 10.1016/j.ultras.2010.01.008.
[56] Jensen J, Olesen JB, Stuart MB, Hansen PM, Nielsen MB, Jensen JA. Vector velocity volume flow estimation: sources of error and corrections applied for arteriovenous fistulas. Ultrasonics 2016;70:136–46. doi: 10.1016/j.ultras.2016.04.023.
[57] Park JH, Choi W, Lee SJ. Adaptive hybrid flow measurement of color Doppler and speckle image velocimetry. Ultrasonics 2020;104:106093. doi: 10.1016/j.ultras.2020.106093.
[58] Brandt AH, Olesen JB, Moshavegh R, Jensen JA, Nielsen MB, Hansen KL. Common carotid artery volume flow: a comparison study between ultrasound vector flow imaging and phase contrast magnetic resonance imaging. Neurol Int 2021;13:269–78. doi: 10.3390/neurolint13030028.
[59] Du Y, Ding H, He L, Deng L, Yu ACH, Yiu BYS, et al. Ultrasound vector flow imaging compared with phase contrast magnetic resonance imaging for estimating blood flow velocity and volume flow in the common carotid artery. 2021 IEEE International Ultrasonics Symposium (IUS); 2021. p. 1–4. doi: 10.1109/IUS52206.2021.9593768.
[60] Kirsanov RI, Kulikov VP. Helical blood flow in hemodynamically significant carotid stenosis. J Ultrasound Med 2020;39:543–50. doi: 10.1002/jum.15131.
[61] Marshall I, Zhao S, Papathanasopoulou P, Hoskins P, Xu XY. MRI and CFD studies of pulsatile flow in healthy and stenosed carotid bifurcation models. J Biomech 2004;37:679–87. doi: 10.1016/j.jbiomech.2003.09.032.
[62] Gharahi H, Zambrano BA, Zhu DC, DeMarco JK, Baek S. Computational fluid dynamic simulation of human carotid artery bifurcation based on anatomy and volumetric blood flow rate measured with magnetic resonance imaging. Int J Adv Eng Sci Appl Math 2016;8:46–60. doi: 10.1007/s12572-016-0161-6.
[63] Lewis P, Psaila JV, Morgan RH, Davies WT, Woodcock JP. Common femoral artery volume flow in peripheral vascular disease. Br J Surg 1990;77:183–7. doi: 10.1002/bjs.1800770220.
[64] Osada T. Physiological aspects of the determination of comprehensive arterial inflows in the lower abdomen assessed by Doppler ultrasound. Cardiovasc Ultrasound 2012;10:13. doi: 10.1186/1476-7120-10-13.
[65] Leszczyński J, Kaszczewski P, Elwertowski M, Stępkowski K, Maciąg R, Elwertowska A, et al. Volumetric flow changes in extracranial arteries in a symptomatic patient with significant bilateral carotid artery stenosis: a case study and literature review. Am J Case Rep 2020;21 0–0. doi: 10.12659/AJCR.927202.
[66] Hungerford SL, Song N, Loo B, Sritharan H, Rye E, Everett K, et al. The effect of increased vascular afterload measures on flow rate and survival in severe aortic stenosis. Eur Heart J - Cardiovasc Imaging 2025;26:674–85. doi: 10.1093/ehjci/jeae331.
[67] Rossi S, Ramalli A, Fool F, Tortoli P. High-frame-rate 3-D vector flow imaging in the frequency domain. Appl Sci 2020;10:5365. doi: 10.3390/app10155365.